HEFAT2007
5th International Conference on Heat Transfer, Fluid Mechanics and Thermodynamics
Sun City, South Africa
Paper number: K10

PREDICTION OF FLOW BOILING HEAT TRANSFER OF CARBON DIOXIDE INSIDE SMALL DIAMETER TUBES

John R. Thome
Laboratory of Heat and Mass Transfer, École Polytechnique Fédérale de Lausanne
EPFL-STI-ISE-LTCM, Mail 9, CH-1015 Lausanne, Switzerland
e-mail: john.thome@epfl.ch

ABSTRACT

This paper reviews recent experimental work on intube flow boiling of carbon dioxide and describes the updated flow boiling heat transfer model and flow pattern map proposed by Cheng, Ribatski, Wojtan and Thome [1] for evaporation of carbon dioxide in small diameter horizontal tubes. This new flow boiling heat transfer model predicted 76% of the CO_2 database taken from the literature within ±30%. The new model and map are applicable to: tube diameters from 0.8 to 10 mm, mass velocities from 170 to 570 kg/m^{2}s, heat fluxes from 5 to 32 kW/m^2 and saturation temperatures from -28°C to 25°C (reduced pressures from 0.21 to 0.87). Simulations of the flow pattern map and heat transfer model are also shown.

NOMENCLATURE

c_p	[J/kgK]	specific heat at constant pressure
D	[m]	internal tube diameter
D_{eq}	[m]	equivalent diameter
D_{ref}	[m]	reference diameter
Fr	[-]	Froude number $[G^2/(\rho^2 gD)]$
G	[kg/m^{2}s]	total vapor and liquid two-phase mass flux
g	[m/s^2]	gravitational acceleration
h	[W/m^{2}K]	heat transfer coefficient,
k	[W/mK]	thermal conductivity,
M	[kg/kmol]	molecular weight
Pr	[-]	Prandtl number $[c_p\mu/k]$
p	[Pa]	pressure
p_r	[-]	reduced pressure $[p/p_{crit}]$
q	[W/m^2]	heat flux
Re_H	[-]	homogeneous Reynolds number $[(GD/\mu_V)x\rho_V/\rho_L(1-x)]$
Re_V	[-]	vapor phase Reynolds number $[GxD/(\mu_V\varepsilon)]$
S	[-]	nucleate boiling suppression factor
T	[°C]	temperature
We	[-]	Weber number $[G^2D/(\rho\sigma)]$
x	[-]	vapor quality
Y	[-]	correction factor

Greek symbols

δ	[m]	liquid film thickness
ε	[-]	cross-sectional vapor void fraction
μ	[Ns/m^2]	dynamic viscosity
θ	[rad]	angle of tube perimeter
ρ	[kg/m^3]	density
σ	[N/m]	surface tension

Subscripts

cb	convection boiling
crit	critical
de	dryout completion
di	dryout inception
dry	dry
dryout	dryout region
exp	experimental
IA	intermittent flow to annular flow
L	liquid
mist	mist flow
nb	nucleate boiling
pred	predicted
sat	saturation
strat	stratified flow
tp	two-phase flow
V	vapor
wavy	wavy flow
wet	on the wet perimeter

INTRODUCTION

Carbon dioxide is receiving a lot of attention as an environmentally safe refrigerant for various applications: automotive air conditioning, low temperature refrigeration systems and hot water heat pumps. Because of its low critical temperature (31.1°C) and high critical pressure (73.8 bar) relative to other widely used refrigerants, CO_2 is utilized at much higher operating pressures than typical of other refrigerants, which results in a significant extrapolation of conventional flow pattern maps and flow boiling models when applied to CO_2, resulting typically in *very* poor accuracy. In brief, the reason for this is that CO_2 has much larger nucleate boiling heat transfer coefficients than conventional refrigerants at the same saturation temperature. Consequently, its nucleate boiling coefficients are often much larger than their corresponding convective heat transfer coefficients at low vapor qualities, which is the inverse of the situation for commonly used refrigerants. Experimental studies have also demonstrated that the onset of dryout is reached earlier for CO_2 during flow boiling, which is particularly important when designing direct-expansion evaporators. Furthermore, discrepancies between flow patterns observed for CO_2 compared with the flow pattern maps for low pressure refrigerants have been observed as well.

Thome and Ribatski [2] recently reviewed the CO_2 flow boiling heat transfer and two-phase flow literature. They addressed the experimental studies on heat transfer and two-phase flow in macro-channels and micro-channels, macro- and micro-scale heat transfer prediction methods for CO_2, and comparisons of these methods to an experimental database extracted from the same literature. CO_2 flow pattern observations were also compared to some of the leading flow pattern maps. They arbitrarily adopted a diameter of 3 mm to segregate the databases and heat transfer models into macro-channels and micro-channels. The CO_2 prediction methods by Wang et al. [3], Yoon et al. [4] and Yoon et al. [5] failed to predict most of the macro-channel flow boiling experimental data while the CO_2 method proposed by Thome and El Hajal [6] predicted reasonably well the newer macro-scale database of CO_2 only at low vapor qualities. They also found that both micro-scale and macro-scale prediction methods performed poorly when compared against independent small diameter data.

NEW THOME AND COWORKERS CO_2 FLOW PATTERN MAP

Consequently, Cheng et al. [1] proposed an updated flow pattern map and flow boiling model for CO_2 that will be described and discussed in this keynote lecture. The experimental conditions of their CO_2 flow boiling database included experimental results from six independent studies obtained for mass velocities from 80 to 570 kg/m^{2}s, heat fluxes from 5 to 32.06 kW/m^2, saturation temperatures from –28 to 25^{o}C (reduced pressures from 0.21 to 0.87) and tube diameters from 0.8 to 10.06 mm. All experiments were for horizontal tubes. Their new heat transfer model and flow pattern map were developed specially for CO_2. As the starting point, the conventional refrigerant models developed by Wojtan et al. [7,8] were used, which are updated versions of the flow pattern map and flow boiling heat transfer model of Kattan et al. [9,10] and Thome and El Hajal [6]. The new method includes a new correlation for the nucleate boiling heat transfer derived from flow boiling data at low vapor quality and introduces a boiling suppression factor in the heat transfer model. In addition, a new dryout inception vapor quality correlation was proposed for CO_2 and accordingly the heat transfer predictions in the dryout region were improved by better identification of this regime's boundary in the new map.

The new flow pattern map for CO_2 of Cheng et al. [1] was developed according to the corresponding heat transfer mechanisms in the various flow regimes. Based on their heat transfer database (not flow pattern observations that are quite limited for CO_2), the intermittent flow to annular flow transition (I-A) and the annular flow to dryout region transition (A-D) criteria in the flow pattern map of Wojtan et al. [7] were modified to fit the experimental data of CO_2. Thus, their new flow pattern map is directly related to the corresponding heat transfer mechanisms and trends of CO_2. The other transition criteria remained the same as in Wotjan et al. [7] and are not discussed further here.

To reflect the real mass flow velocities for non-circular channels, equivalent diameters D_{eq} are used for non-circular channels rather than hydraulic diameters in the flow pattern map and flow boiling model, the latter which seem to have no physical relationship to an annular film flow for instance. The equivalent diameter is that of a circular channel with the same cross-sectional area as the non-circular channel, such that the mass velocities remain the same in both channels (this is not true when using the hydraulic diameter). Furthermore, when using a void fraction equation to calculate mean velocities of the phases as is done in the present methods, these remain the same in an equivalent diameter tube as in the non-circular tube but do *not* when applying the hydraulic diameter tube definition to two-phase flows.

Flow pattern transitions under diabatic flow boiling conditions are, in part, intrinsically related to the changes in trends in flow boiling heat transfer coefficients. This means that flow pattern maps can be used to explain the characteristics of flow boiling data and vice versa. Specifically in the present case, CO_2 depicts strong nucleate boiling heat transfer characteristics in intermittent flow at low vapor quality due to its high reduced pressure. The distinction between intermittent (I) flow and annular (A) flow was indicated by the sharp decline of the heat transfer coefficient data between the two flow regimes. The entrance into the dryout region (D) is also quite evident by the sharp drop in heat transfer when the top of a horizontal tube becomes dry, where the fraction of the perimeter then grows with increasing vapor quality until the entire perimeter is dry and mist flow is encountered, with yet another characteristic change in trend in the heat transfer data. Therefore, the distinction between annular flow and dryout region was determined by analysis of the heat transfer database.

Based on the experimental heat transfer data, the following new transition criteria were proposed for CO_2:

1. The I-A transition boundary was calculated with its new criterion as follows:

$$x_{IA} = \left[1.8^{1/0.875}\left(\rho_V/\rho_L\right)^{-1/1.75}\left(\mu_L/\mu_V\right)^{-1/7}+1\right]^{-1} \quad (1)$$

2. The A-D transition boundary was calculated with its new criterion as follows:

$$G_{dryout} = \left\{\frac{1}{0.67}\left[\ln\left(\frac{0.58}{x}\right)+0.52\right]\left(\frac{D}{\rho_V\sigma}\right)^{-0.17}\left[\frac{1}{gD\rho_V(\rho_L-\rho_V)}\right]^{-0.348}\left(\frac{\rho_V}{\rho_L}\right)^{-0.25}\left(\frac{q}{q_{crit}}\right)^{-0.7}\right\}^{0.965} \quad (2)$$

The new onset of dryout inception vapor quality x_{di} that marks the transition from annular flow to dryout is predicted as:

$$x_{di} = 0.58e^{\left[0.52-0.67We_V^{0.17}Fr_V^{0.348}\left(\rho_V/\rho_L\right)^{0.25}\left(q/q_{crit}\right)^{0.7}\right]} \quad (3)$$

In this equation, q_{crit} is calculated according to Kutateladze [11].

Figure 1 (top) shows the comparison of the new flow pattern map for CO_2 and the flow pattern map of Wojtan et al. to the experimental data of Yun et al. [12] at the indicated test conditions. In the flow pattern map, **A** stands for annular flow, **D** stands for the dryout region, **I** stands for intermittent flow, **M** stands for mist flow, **S** stands for stratified flow and

SW stands for stratified-wavy flow. The stratified to stratified-wavy flow transition is designated as S-SW, the stratified-wavy to intermittent/annular flow transition is designated as SW-I/A, the intermittent to annular flow transition is designated as I-A and so on. The arrows show the changes of I-A, A-D and S-SW/Slug+SW transition boundaries made for CO_2. Figure 1 (bottom) shows the corresponding comparison of the predicted heat transfer coefficients with the heat transfer model of Wojtan et al. and the new heat transfer model (described below) for CO_2 to the experimental data at the same conditions. Obviously, the flow pattern map of Wojtan et al. did not reflect the sharp changes in trends in CO_2 heat transfer correctly and the heat transfer model for conventional refrigerants of Wojtan et al. predicted poorly the experimental heat transfer coefficients of CO_2. The new CO_2 flow pattern map thus helps the flow boiling heat transfer model to capture the location of the sharp fall off in heat transfer at the onset of dryout at the top of the tube and thus improves both the accuracy and reliability of the new heat transfer model.

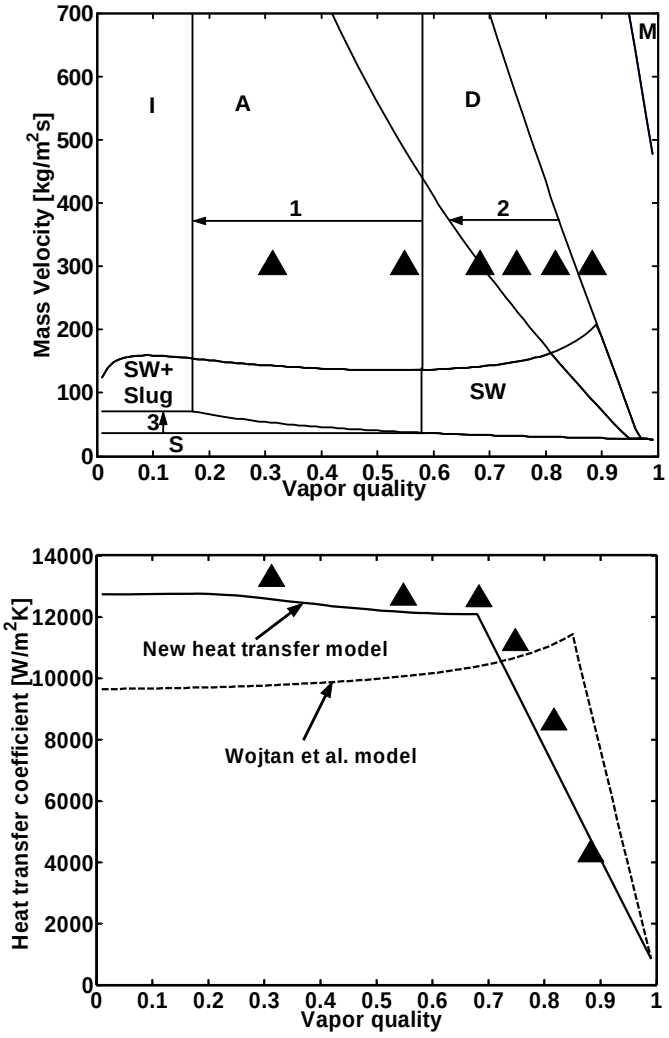

Figure 1 New flow pattern map (top) and heat transfer data (bottom) of Yun et al. [12] for CO_2 for D = 1.54 mm, G = 300 kg/m^{2}s, T_{sat} = 5 °C and q = 20 kW/m^2. *Arrow 1* shows the change of I-A transition boundary, *arrow 2* the change of A-D transition boundary and *arrow 3* the change of S-SW/SW+Slug boundary.

NEW THOME AND COWORKERS FLOW BOILING HEAT TRANSFER MODEL FOR CO_2

It is a formidable challenge to develop a general flow boiling heat transfer model for CO_2 because of the significant diversities of the heat transfer trends in the database from study to study. Since such a method will be used to optimize the configuration and size of CO_2 evaporators, it is important that it is not only statistically accurate but that it captures correctly the trends in the data and in particular the locations of the sharp changes in heat transfer. Most importantly, the heat transfer mechanisms should be related to the corresponding flow patterns and be physically explained according to flow pattern transitions. Accordingly, Cheng et al. [1] proposed a new general heat transfer model for CO_2 using the Wojtan et al. [8] model as the starting point.

Brief description of the flow boiling heat transfer model of Wojtan et al.

Wojtan et al. [8] extended the Kattan et al. [10] heat transfer model to include a dryout region and methods to predict heat transfer in the dryout and mist flow regimes while also improving the heat transfer methods for stratified-wavy flows by dividing that regime into three sub-regimes. The Kattan-Thome-Favrat general equation for the local heat transfer coefficients h_{tp} in a horizontal tube is:

$$h_{tp} = \left[\theta_{dry} h_V + \left(2\pi - \theta_{dry}\right) h_{wet}\right] / 2\pi \qquad (4)$$

where θ_{dry} is the dry angle as shown in Figure 2. The dry angle is used in defining the basic two-phase flow structures and the ratio of the tube perimeters in contact with liquid and vapor. In stratified flow, θ_{dry} equals the stratified angle, θ_{strat}, which is calculated according to the method in Thome and El Hajal [6]. In annular and intermittent flows, θ_{dry} = 0. For stratified-wavy flow, θ_{dry} varies from zero up to its maximum value θ_{strat}. Wojtan et al. subdivided the stratified-wavy flow into three subzones (slug, slug/stratified-wavy and stratified-wavy). Based on the fact that the high frequency slugs maintain a continuous thin liquid layer on the upper tube perimeter, θ_{dry} is defined equal to 0 in the slug zone. The dry angles in the slug/stratified-wavy and stratified-wavy regions are calculated according to equations developed by Wojtan et al. based in exponential interpolations giving smooth transition in the determination of the dry angle between the respective zones and also a smooth transition in the heat transfer coefficient from zone to zone.

The vapor phase heat transfer coefficient on the dry perimeter h_V is calculated with the Dittus-Boelter [13] correlation assuming tubular flow in the tube:

$$h_V = 0.023\, Re_V^{0.8}\, Pr_V^{0.4} \left(k_V / D\right) \qquad (5)$$

and the heat transfer coefficient on the wet perimeter is calculated with an asymptotic model that combines the nucleate boiling and convective boiling contributions to the heat transfer by the third power:

$$h_{wet} = \left[\left(h_{nb}\right)^3 + h_{cb}^{\,3}\right]^{1/3} \qquad (6)$$

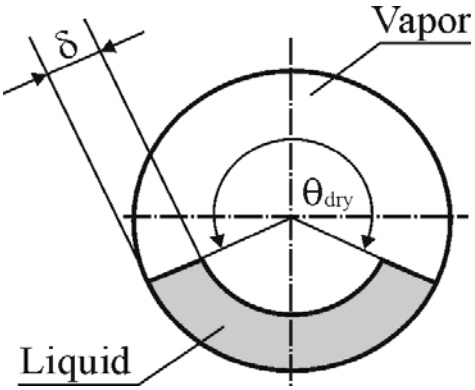

Figure 2 Schematic diagram of annular flow with partial dryout.

In this equation, the correlation proposed by Cooper [14] multiplied by a fixed boiling suppression factor of 0.8 was used to calculate the nucleate boiling contribution. The convective contribution was calculated as in the original Kattan et al. correlation assuming a liquid film flow:

$$h_{cb} = 0.0133\left(\frac{4G(1-x)\delta}{\mu_L(1-\varepsilon)}\right)^{0.69} Pr_L^{0.4}\,\frac{k_L}{\delta} \qquad (7)$$

The term in the bracket is the liquid film Reynolds number.

The void fraction ε is determined with the Rouhani and Axelsson [15] drift flux model and the liquid film thickness from the geometry in Fig. (2), as was done in the model of Wojtan et al.

The heat transfer coefficient in mist flow h_{mist} is calculated in the Wojtan et al. model using the following correlation:

$$h_{mist} = 0.0117\,Re_H^{0.79}\,Pr_V^{1.06}\,Y^{-1.83}(k_V/D) \qquad (8)$$

where Re_H is the homogeneous Reynolds number and Y is the correction factor originally proposed by Groeneveld [16] and given by:

$$Y = 1 - 0.1\left[(\rho_L/\rho_V - 1)(1-x)\right]^{0.4} \qquad (9)$$

The heat transfer coefficient in the dryout region along a horizontal channel is calculated by proration as:

$$h_{dryout} = h_{tp}(x_{di}) - \frac{x - x_{di}}{x_{de} - x_{di}}\left[h_{tp}(x_{di}) - h_{mist}(x_{de})\right] \qquad (10)$$

In this expression, $h_{tp}(x_{di})$ is the two-phase flow heat transfer coefficient calculated from Eq. (4) at the dryout inception quality x_{di} and $h_{mist}(x_{de})$ is the mist flow heat transfer coefficient calculated from Eq. (8) at the dryout completion quality x_{de}. If x_{de} is calculated to be larger than 0.999, then x_{de} is reset to 0.999. For more details and complete set of equations for the flow boiling heat transfer model and flow patterns map of Wotjan et al., refer to the original papers.

Modifications in the new flow boiling heat transfer model for CO_2

Like other flow boiling heat transfer models, both the original Kattan-Thome-Favrat model and the modified model of Wojtan et al. significantly under predict the flow boiling heat transfer coefficients for CO_2, particularly at low and intermediate vapor qualities. Interestingly, CO_2 heat transfer data at high saturation pressures typically show a monotonic decrease versus vapor quality in annular flows, which is the exact opposite of the trend for other refrigerants such as R134a at low pressures. Furthermore, the nucleate boiling contribution is often much larger than the convective boiling contribution for CO_2 while the opposite is true for R-134a. Hence, the suppression of nucleate boiling that could be neglected in the asymptotic method for conventional refrigerants at low pressures cannot be neglected for CO_2, where suppression of nucleate boiling greatly reduces its contribution to the heat transfer with increasing vapor quality.

Therefore, first Cheng et al. [1] developed a new nucleate boiling heat transfer correlation, found to be necessary for CO_2, and then a new boiling suppression factor S was proposed for CO_2. Furthermore, a new correlation for the onset of dryout inception was needed and is given by Eq. (3), in order to predict heat transfer in the dryout region by considering the fact that the onset of dryout of CO_2 occurs much earlier than for other refrigerants.

Nucleate boiling heat transfer correlation for CO_2. The experimental flow boiling heat transfer data at vapor qualities $x < x_{IA}$ in the CO_2 database were used to extract the nucleate boiling contribution by removing their convective heat transfer contributions using the above equations to develop a nucleate boiling database for CO_2. The Cooper [14] correlation was found to greatly under predict these data at low heat fluxes while the correlation of Gorenflo [17] over predicted the data by a large margin, where the reason could be the lack of an extensive database for pool boiling of CO_2 in setting his standardized value for CO_2. Thus, the following new nucleate boiling heat transfer correlation for CO_2 was proposed by Cheng et al.:

$$h_{nb} = 131 p_r^{-0.0063}\left(-\log_{10} p_r\right)^{-0.55} M^{-0.5} q^{0.58} \qquad (11)$$

Figure 3 shows the comparison of these "nucleate boiling heat transfer coefficients" by the new nucleate boiling heat transfer correlation for CO_2, where about 90% of the data are predicted within ± 20%.

Nucleate boiling suppression factor correlation for CO_2. As nucleate boiling heat transfer is suppressed by the sharper temperature gradient in the liquid film in an annular flow as per the theory of Chen [18], a boiling suppression factor correlation is needed in the flow boiling heat transfer model for CO_2 to capture the effect. Unlike other earlier boiling suppression factor correlations, which were empirically correlated based on the Lockhart-Martinelli number, Reynolds number, Boiling number and Prandt number, the liquid film thickness was used as a main parameter by Cheng et al. since it was found by analysis of their data to have a significant effect on the values of S back-calculated out of their flow boiling database as follows. First, the Cooper correlation was first replaced with the new nucleate boiling heat transfer correlation. Then, the boiling suppression factors were backed out of the whole database

(except the dryout data points) using the above expressions. Incorporating the effect of tube diameter found during the analysis, the following boiling suppression factor correlation was obtained for CO_2:

If $x < x_{IA}$:

$$S = 1 \tag{12}$$

If $x \geq x_{IA}$:

$$S = 1 - 1.14\left(D/D_{ref}\right)^2\left(1-\delta/\delta_{IA}\right)^{2.2} \tag{13}$$

where D_{ref} = 0.00753m. If D > 7.53 mm, then D is set equal to 7.53 mm. The correlation is applicable to the conditions: -28°C ≤ T_{sat} ≤ 25°C, 5 kW/m^2 ≤ q ≤ 32 kW/m^2, 170 kg/m^{2}s ≤ G ≤ 570 kg/m^{2}s, and 0.8 mm ≤ D ≤ 10 mm.

Combining the nucleate boiling heat transfer correlation for CO_2 and the nucleate boiling heat transfer suppression factor correlation, the flow boiling heat transfer coefficients on the wet perimeter are now calculated as:

$$h_{wet} = \left[\left(S \cdot h_{nb}\right)^3 + h_{cb}{}^3\right]^{1/3} \tag{14}$$

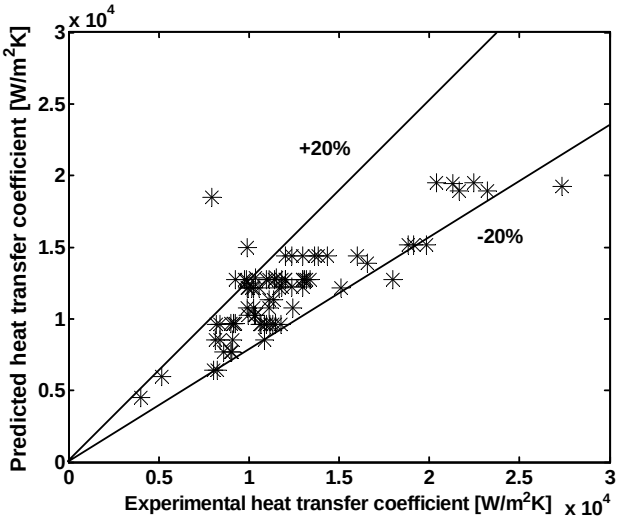

Figure 3 Comparison of their nucleate boiling heat transfer correlation for CO_2 with their database.

Dryout region heat transfer correlation for CO_2. When developing their boiling suppression factor correlation, dryout data were determined according to the corresponding boiling suppression factors. Those giving negative boiling suppression factor values were taken as dryout data points and the data giving boiling suppression factor values around zero were taken as indicating the location of the onset of the dryout. Based on these dryout inception data, the dryout inception vapor quality correlation of Wojtan et al. was modified and thus a new annular to dryout region (A-D) transition boundary in the flow pattern map was extracted for CO_2. By comparing the new flow pattern map with the experimental data, the dryout inception vapor quality correlation was modified and is given by Equations (2) and (3) presented earlier.

COMPARISONS OF NEW HEAT TRANSFER MODEL TO DATABASE

Figures 4 and 5 show several of their comparisons of the new flow boiling heat transfer model to a selection of experimental heat transfer coefficients, which is seen to not only predict the experimental heat transfer coefficients well but also to capture the trends of the experimental heat transfer coefficients. Statistically, 75.5% of the entire database was predicted within ± 30% using the new Cheng et al. flow pattern map and flow boiling model for CO_2. For such a wide range of experimental data from different laboratories, especially covering the difficult dryout, mist and stratified-wavy flow regimes, the updated methods are shown to work quite well. As even more CO_2 data have become available since the work on Cheng et al. [1] study was completed in 2005, Thome and coworkers are implementing further improvements to the methods presented here and hope to have an even more accurate, more reliable method that covers a larger range of test conditions available in 2007.

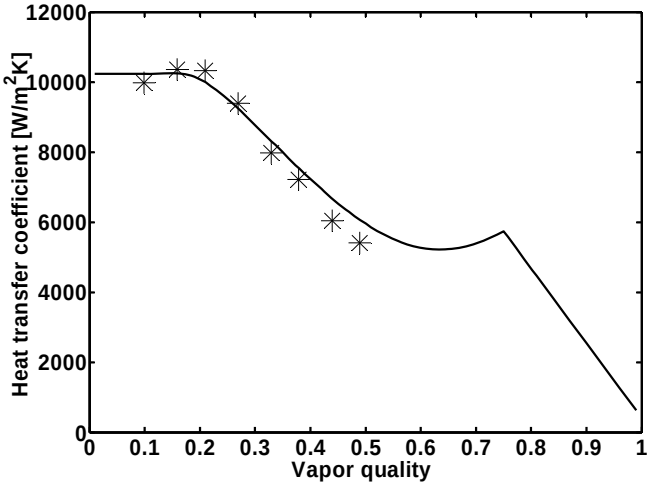

Figure 4 Comparison of the predicted flow boiling heat transfer coefficients with the experimental flow boiling heat transfer coefficients of Yoon et al. [4] for D = 7.35 mm, T_{sat} = 0 °C, G = 318 kg/m^{2}s, q = 16.4 kW/m^2.

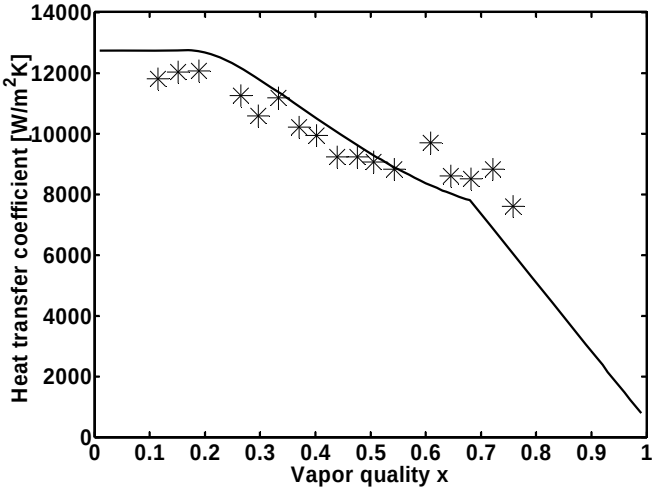

Figure 5 Comparison of the predicted flow boiling heat transfer coefficients with the experimental flow boiling heat transfer coefficients of Yun et al. [20] for D = 6 mm , T_{sat} = 5 °C, G = 340 kg/m^{2}s, q = 20 kW/m^2.

Figure 6 shows a simulation of the new flow pattern map and flow boiling model for CO_2 calculated for a 7 mm channel at a heat flux of 10 kW/m^2, a saturation temperature of -20°C and a mass velocity of 400 kg/m^{2}s, superimposed on the same graph using the calculator embedded within the newest version of the e-book of Thome [19]. The process path for the vapor quality variation from x = 0.01 to x = 0.99 is shown as the broken red line while the variation in the heat transfer coefficient as it changes vapor quality and flow pattern is depicted by the solid red line. The flow pattern boundaries are in black. Notice the various changes in trends in the heat transfer coefficient as this occurs. For example, when the flow regime passes from annular flow into the dryout regime there is a sharp inflection in the heat transfer coefficient as the top perimeter of the tube becomes dry and dryout progresses around the perimeter with increasing vapor quality.

Figure 7 similarly depicts another simulation for a 7 mm channel at the following conditions: q = 5 kW/m^2, T_{sat} = 10°C and G = 200 kg/m^{2}s. At this condition that the slug flow regime disappears (the black curved line within the slug+SW region is the continuation of the G_{wavy} transition line, which is below the horizontal upper boundary of this latter regime and hence the slug regime does not appear in the map).

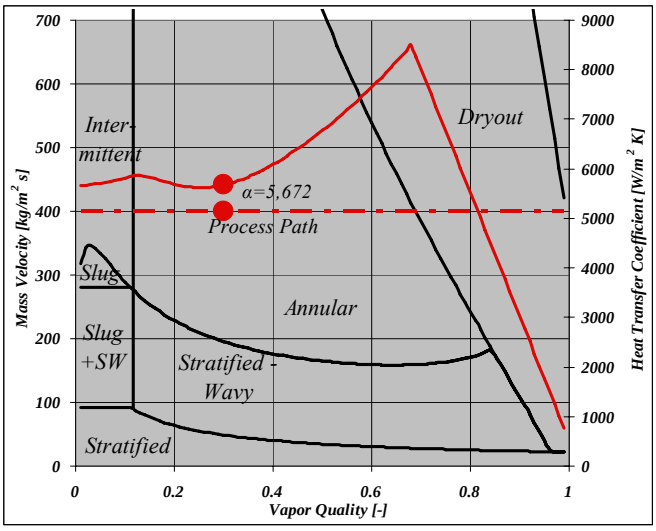

Figure 6 Simulation of flow boiling model and flow pattern map for 7 mm channel at following conditions: q = 10 kW/m^2, T_{sat} at -20°C and G = 400 kg/m^{2}s with indicated value at x = 0.30.

CONCLUSIONS

This keynote lecture has described the updated flow boiling heat transfer model and flow pattern map for two-phase flow in horizontal tubes that has been developed specifically for CO_2 by Cheng et al. [1]. The new flow boiling heat transfer model and map include a new nucleate boiling heat transfer correlation for CO_2, a new nucleate boiling suppression factor correlation for CO_2 and a new dryout inception vapor quality correlation for CO_2. The new heat transfer model predicts 75.5% of the CO_2 database (318 data points) to within ± 30%. The heat transfer model and the corresponding flow pattern map are applicable to quite a wide range of conditions: tube diameters (equivalent diameter for non-circular channels) from 0.8 to 10 mm, mass velocities from 170 to 570 kg/m^{2}s, heat fluxes from 5 to 32 kW/m^2 and saturation temperatures from –25°C to +25°C.

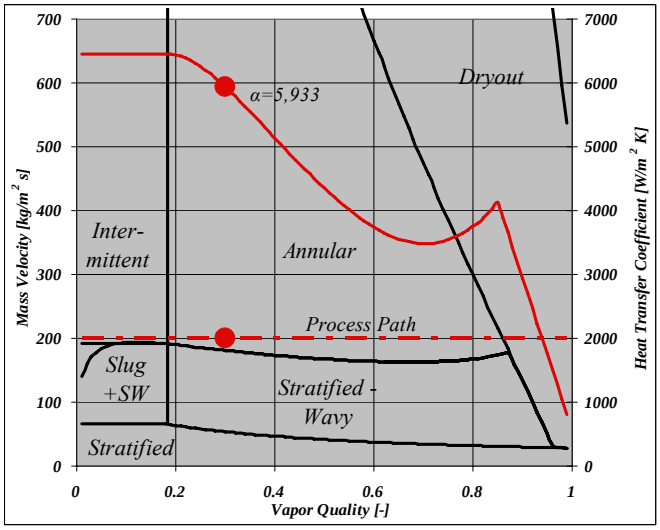

Figure 7 Simulation of flow boiling model and flow pattern map for 7 mm channel at following conditions: q = 5 kW/m^2, T_{sat} at 10°C and G = 200 kg/m^{2}s with indicated value at x = 0.30.

REFERENCES

1. Cheng, L., Ribatski, G., Wojtan, L. and Thome, J.R., 2006, New Flow Boiling Heat Transfer Model and Flow Pattern Map for Carbon Dioxide Evaporating inside Tubes, *Int. J. Heat Mass Transfer*, Vol. 49, pp. 4082-4094.
2. Thome, J.R. and Ribatski, G., 2006, State-of-the Art of Flow Boiling and Two-Phase Flow of CO_2 in Macro- and Micro-Channels, *Int. J. Refrigeration*, Vol. 28, pp. 1149-1168.
3. Wang, J., Ogasawara, S. and Hihara, E., 2003, Boiling Heat Transfer and Air Coil Evaporator of Carbon Dioxide, 21st IIR International Congress of Refrigeration, Washington DC, paper ICR0231.
4. Yoon, S.H, Cho, E.S., Hwang, Y.W., Kim, M.S., Min, K. and Kim, Y., 2004, Characteristics of Evaporative Heat Transfer and Pressure Drop of Carbon Dioxide and Correlation Development, *Int. J. Refrigeration*, Vol. 27, pp. 111-119.
5. Yoon, S.H, Cho, E.S., Kim, M.S. and Kim, Y., 2003, Studies on the Evaporative Heat Transfer and Pressure Drop of Carbon Dioxide near the Critical Point, 21st IIR International Congress of Refrigeration, Washington DC, paper ICR0477.
6. Thome, J.R. and El Hajal, J., 2004, Flow Boiling Heat Transfer to Carbon Dioxide: General Prediction Method, *Int. J. Refrigeration*, Vol. 27, pp. 294-301.
7. Wojtan, L., Ursenbacher, T., and Thome, J.R., 2005a, Investigation of Flow Boiling in Horizontal Tubes: Part I – A New Diabatic Two-Phase Flow Pattern Map, *Int. J. Heat Mass Transfer*, Vol. 48, pp. 2955-2969.
8. Wojtan, L., Ursenbacher, T., and Thome, J.R., 2005b, Investigation of Flow Boiling in Horizontal Tubes: Part II – Development of a New Heat Transfer Model for

Stratified-Wavy, Dryout and Mist Flow Regimes, *Int. J. Heat Mass Transfer*, Vol. 48, pp. 2970-2985.
9. Kattan, N., Thome, J.R. and Favrat, D., 1998, Flow Boiling in Horizontal Tubes. Part 1: Development of a Diabatic Two-Phase Flow Pattern Map, *J. Heat Transfer*, Vol. 120, pp. 140-147.
10. Kattan, N., Thome, J.R. and Favrat, D., 1998, Flow Boiling in Horizontal Tubes: Part-3: Development of a New Heat Transfer Model Based on Flow Patterns, *J. Heat Transfer*, Vol. 120, pp. 156-165.
11. Kutateladze, S.S., 1948, On the Transition to Film Boiling under Natural Convection, *Kotloturbostroenie*, Vol. 3, pp. 10-12.
12. Yun, R., Kim, Y. and Kim, M.S., 2005, Convective Boiling Heat Transfer Characteristics of CO_2 in Microchannels, *Int. J. Heat Mass Transfer*, Vol. 48, pp. 235-242.
13. Dittus, F.W. and Boelter, L.M.K., 1930, Heat Transfer in Automobile Radiator of the Tubular Type, *Univ. Calif. Publ. Eng.*, Vol. 2(13), pp. 443-461.
14. Cooper, M.G., 1984, Heat Flow Rates in Saturated Nucleate Pool Boiling - A Wide-Ranging Examination of Reduced Properties, *Advances in Heat Transfer*, Vol. 16, pp. 157–239.
15. Rouhani, Z. and Axelsson, E., 1970, Calculation of Volume Void Fraction in a Subcooled and Quality Region, *Int. J. Heat Mass Transfer*, Vol. 17, pp. 383-393.
16. Groeneveld, D.C., 1973, Post Dryout Heat Transfer at Reactor Operating Conditions, ANS Topical Meeting on Water Reactor Safety, Salt Lake City.
17. Gorenflo, D., 1993, Pool Boiling, Chapter Ha,*VDI Heat Atlas*, Düsseldorf: VDI-Verlag.
18. Chen, J.C., 1966, Correlation for Boiling Heat-Transfer to Saturated Fluids in Convective Flow, *Ind. Chem. Eng. Proc. Des. Dev.*, Vol. 5, pp. 322-339.
19. Thome, J.R.,2006, Wolverine Engineering Databook III Calculator, *Wolverine Engineering Databook III*, available for free at following website: http://www.wlv.com/products/databook/db3/DataBookIII.pdf.
20. Yun, R., Kim, Y., Kim, M.S. and Choi, Y., 2003, Boiling Heat Transfer and Dryout Phenomenon of CO_2 in a Horizontal Smooth Tube, *Int. J. Heat Mass Transfer*, Vol. 46, pp. 2353-2361.